STRESS DISTRIBUTION IN THE CANINE LEFT VENTRICLE DURING DIASTOLE AND SYSTOLE

DANIEL D. STREETER, JR., RAMESH N. VAISHNAV, DALI J. PATEL, HENRY M. SPOTNITZ, JOHN ROSS, JR., *and* EDMUND H. SONNENBLICK

From the Section on Clinical Biophysics and Cardiology Branch, National Heart Institute, National Institutes of Health, Bethesda, Maryland 20014. The present addresses of the authors are as follows: Dr. Streeter, Department of Pathology, University of Washington Medical School, Seattle, Washington 98105; Dr. Vaishnav, Civil Engineering and Mechanics Department, The Catholic University of America, Washington, D. C. 20017; Dr. Spotnitz College of Physicians and Surgeons, Columbia University, New York 10032; Dr. Ross, Department of Medicine, University of California, San Diego, La Jolla, California 92037; Dr. Sonnenblick, Cardiovascular Unit, Peter Bent Bringham Hospital, Boston, Massachusetts 02115.

ABSTRACT A model is proposed for stress analysis of the left ventricular wall (LV wall) based on the realistic assumption that the myocardium is essentially composed of fiber elements which carry only axial tension and vary in orientation through the wall. Stress analysis based on such a model requires an extensive study of muscle fiber orientation and curvature through the myocardium. Accordingly, the principal curvatures were studied at a local site near the equator in ten dog hearts rapidly fixed *in situ* at end diastole and end systole; the fiber orientation for these hearts had already been established in a previous study. The principal radii of curvature were (*a*) measured by fitting templates to the endocardial and epicardial wall surfaces in the circumferential and longitudinal directions and (*b*) computed from measured lengths of semiaxes of ellipsoids of revolution representing the LV wall ("ellipsoid" data). The wall was regarded as a tethered set of nested shells, each having a unique fiber orientation. Results indicate the following. (*a*) Fiber curvature, k, is maximum at midwall at end systole; this peak shifts towards endocardium at end diastole. (*b*) The pressure or radial stress through the wall decreases more rapidly near the endocardium than near the epicardium at end diastole and at end systole when a constant tension is assumed for each fiber through the wall. (*c*) At end diastole the curve for the circumferential stress vs. wall thickness is convex with a maximum at midwall. In the longitudinal direction the stress distribution curve is concave with a minimum at midwall. Similar distributions are obtained at end systole when a constant tension is assumed for each fiber through the wall. (*d*) The curvature and stress distributions obtained by direct measurements at a selected local site agree well with those computed from "ellipsoid" data.

INTRODUCTION

A precise knowledge of stress distribution in the ventricular wall is important to the physiologist for understanding the behavior of ventricular muscle, for building a realistic mathematical model of the heart as a pump, as well as for studying the mechanical behavior of the coronary vascular bed. The ventricular wall is essentially composed of ordered sets of interconnected muscle fibers. The fiber angle (or fiber orientation) through the myocardial wall changes gradually from endocardium to epicardium (Hort, 1960; Streeter and Bassett, 1966; Streeter, Spotnitz, Patel, Ross, and Sonnenblick, 1969). Myocardial-wall stress distribution is then a function of tension, curvature, and spatial orientation of muscle fibers through the wall. In most previous attempts of stress analysis of the myocardium (Woods, 1892; Burton, 1957; Sandler and Dodge, 1963; Wong and Rautaharju, 1968; Hood, Thompson, Rackley, and Rolett, 1969), one of two general approaches have been taken: the first considers the myocardium to be a membrane and the second considers it to be a thick walled structure having isotropic elastic properties. Since both these approaches ignore the role of local fiber geometry, the present analysis was undertaken to incorporate this important factor.

In a recent study (Streeter et al., 1969) the fiber orientation through the left ventricular wall of hearts arrested in diastole and systole has been described. The present study was undertaken (*a*) to measure fiber curvature in the left ventricular wall of these same hearts and (*b*) to calculate myocardial stress distributions using this fiber curvature data together with the fiber orientation data. Since the average reader may be unfamiliar with some of the concepts involved, the relevant theoretical background and mathematical derivations are provided in the Appendix. This presentation will begin with a statement of basic assumptions and then turn to a description of experimental results and their significance.

Basic Assumptions

In this study the myocardium is considered to be a network of interconnected muscle fibers with a preferred orientation that varies radially through the wall. Myocardial fibers are postulated to form a set of nested shells which are interconnected by randomly spaced anastomoses at distances which are large in comparison with the diameter of the muscle fibers, so that the fibers are free to roll or slide over neighboring fibers except at the anastomoses. It is further assumed that the muscle fibers carry only axial tension, are constrained to remain on a shell surface and assume a geodesic[1] configuration. The tensile stress in the direction of a myocardial fiber, according to the hypothesized structural model, depends upon the curvature of the fiber and the pressures acting on their respective areas as shown in Fig. 1 for a simplified case.

[1] A geodesic is a line on a surface of minimum length joining any two points on the surface.

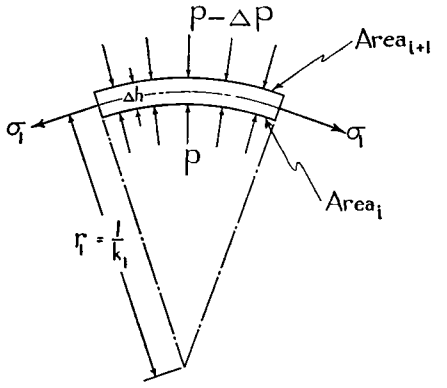

FIGURE 1 Simplified diagram of an element from the middle layer of LV wall where the muscle fibers are circumferentially oriented. For this special case the radial equilibrium equation becomes $pA_i - (p - \Delta p)A_{i+1} \approx k_1\sigma_1 A_i \Delta h$, where p is the pressure on the concave side acting on area A_i, $p - \Delta p$ is the pressure on the convex side acting on area A_{i+1}, Δh is the thickness of the element, σ_1 is the circumferential stress, and k_1 is the curvature of the fiber. The general equation for an arbitrary fiber including the radial acceleration term is derived in the Appendix.

METHODS

Previous studies in this laboratory provided ten dog hearts that had been fixed in the open chest with glutaraldehyde at known phases of the cardiac cycle. These hearts had been used for studies of over-all left ventricular (LV) dimensions (Ross, Sonnenblick, Covell, Kaiser, and Spiro, 1967), midwall sarcomere lengths (Sonnenblick, Ross, Covell, Spotnitz, and Spiro, 1967) and fiber orientation through the wall (Streeter et al., 1969). Of these ten hearts five were fixed at end diastole (mean LV cavity volume 52.4 ± 5.3 SEM ml, mean LV weight 98.6 ± 5.0 g, mean LV midwall sarcomere length 2.07 ± 0.01 μ, mean fixation pressure 11 ± 3 g/cm^2) and five at end systole (mean LV cavity volume 20.6 ± 1.6 ml, mean LV weight 99.4 ± 3.6 g, mean LV midwall sarcomere length 1.84 ± 0.03 μ, mean fixation pressure 143 ± 3 g/cm^2). The criteria used to determine end diastole and end systole for these hearts have been described in detail by Ross et al., (1967). Briefly, end diastole was obtained by first arresting the heart with potassium solution and then adjusting the left atrial pressure to a level approximating the LV end-diastolic pressure observed immediately prior to fixation; the appropriately large cavity volume and midwall sarcomere length verified this state. End systole was indicated on the basis of completed ejection as shown by the arterial pressure pulse, failure of ventricular relaxation as reflected in a delayed down slope of the left ventricular pressure pulse, and appropriately small cavity volume as determined by ventricular casts made after fixation.

"Measured" Data

Since individual myocardial fibers are not visible to the naked eye, the curvature of a fiber, which is the reciprocal of radius of curvature, must be computed from directly measurable quantities such as the principal curvatures[2] of the endocardial and epicardial surfaces. For this purpose, in each heart, a z axis was chosen to pass through the aortic valve commissure between the left and the noncoronary cusps and the apex of the heart. The equatorial plane which is perpendicular to the z axis at the level of maximum LV diameter was then exposed by transection of the LV free wall. A site was selected (site 1, Fig. 2A) within 0.45 cm of the equatorial plane in the LV free wall between the two papillary muscles. On the endo-

[2] For a surface of revolution (see Fig. 2A), the lines of latitude and longitude (parallel circles and meridians, respectively) define the directions of principal curvature and form an orthogonal gridwork on the surface.

cardial and epicardial surfaces of site 1, the local principal radii of curvature in the circumferential direction ($r_{1,1}$ and $r_{1,n}$, respectively) and in the longitudinal direction ($r_{2,1}$ and $r_{2,n}$, respectively) were measured by means of sheet aluminum templates. These templates were cut to radii ranging from 0.5 to 10 cm in increments of 0.5 cm and from 11 to 31 cm in increments of 1 cm with both convex and concave edges. Templates were fitted perpendicularly to a square cm of the local surface along the principal directions (circumferential and

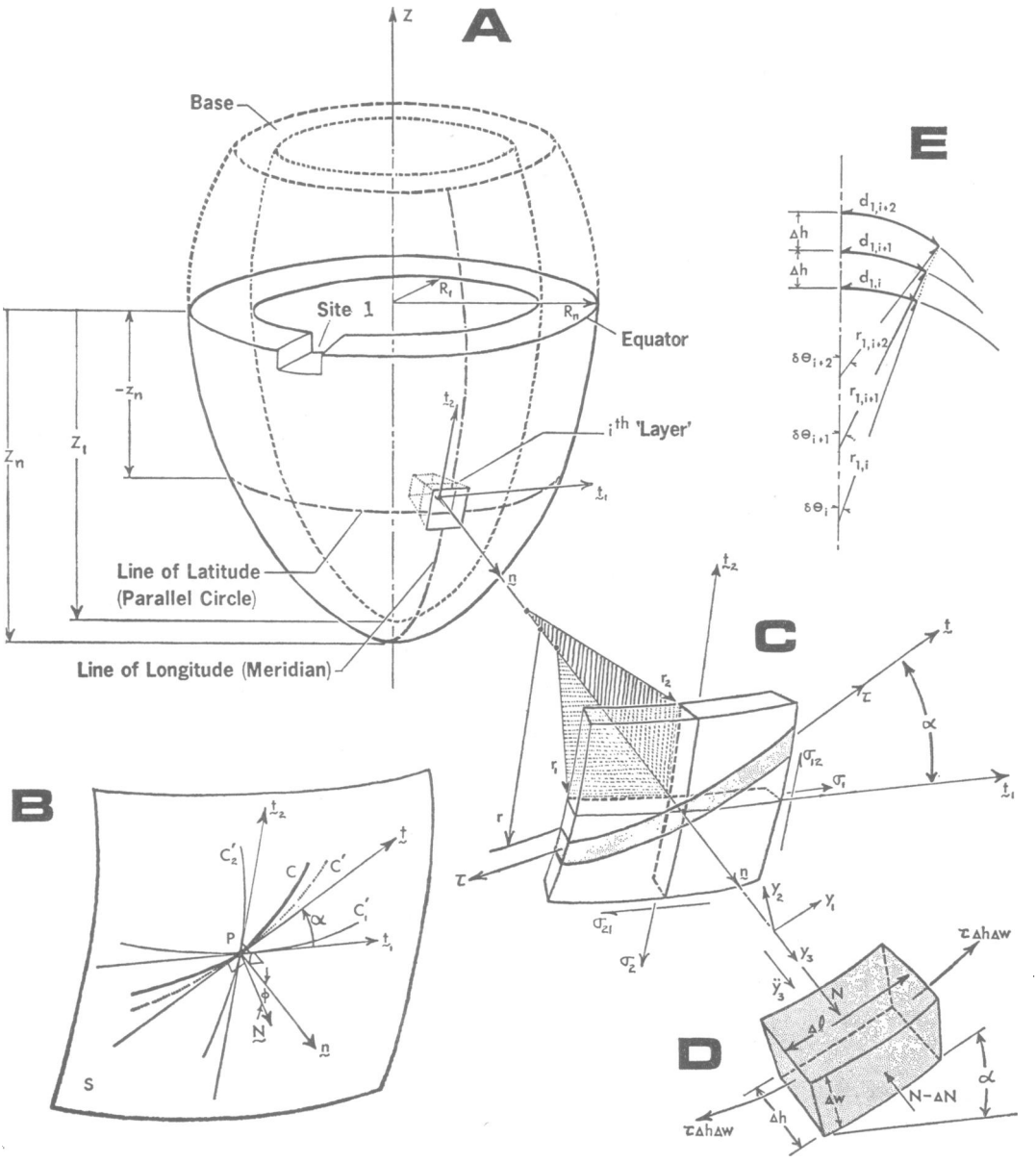

longitudinal) as shown by the two hatched areas in Fig. 2C. At each site the wall thickness, h, was measured by a caliper. All computations based on these data will be referred to as "measured" data.

"Ellipsoid" Data

For an alternate estimate of local curvatures at site 1, the two LV wall surfaces were regarded as truncated ellipsoids of revolution. The minor and major principal semiaxes of the endocardial (R_1 and Z_1, respectively) and epicardial surfaces (R_n and Z_n, respectively) as shown in Fig. 2A, were measured on each heart. Inner diameters were measured in four representative directions which excluded the papillary muscles but did not exclude trabecular protuberances. These same four representative directions were also used in measuring outside diameters. These data were averaged to obtain R_1 and R_n. The axial distances, z_1 and z_n, from the equatorial plane to midpoint of the endocardial and epicardial surfaces respectively of site 1 were also recorded (see Fig. 2A). By using equations

$$r_1 = (Z^2 - [Z^2 - R^2]\, f^2)^{1/2}\, R/Z \tag{1}$$

$$r_2 = (Z^2 - [Z^2 - R^2]\, f^2)^{3/2}/RZ, \tag{2}$$

where $f = z/Z$, the endocardial and epicardial values of the principal radii of curvature ($r_{1,1}$, $r_{2,1}$, $r_{1,r}$, $r_{2,n}$) at site 1 were calculated. All computations based on these data will be referred to as "ellipsoid" data.

Interpolation Procedure

For deducing the radii of curvature of an internal fiber from the above data, the following procedure was used. From the values of R_1, R_n, Z_1 and Z_n, values of R_i and Z_i for intermediate ellipsoids of revolution were computed by linear interpolation, and the corresponding values of $r_{1,i}$ and $r_{2,i}$ were calculated using equations 1 and 2. These values of $r_{1,i}$ and

---

FIGURE 2 Geometry of LV wall.
(A) shows the LV wall as approximated by truncated ellipsoids of revolution. Lines of longitude and latitude define a site that penetrates the wall thickness. Site 1, which was used for data collection, usually straddles the equator. For generality, an arbitrary site not at the equator is shown to illustrate geometrical concepts. $\underset{\sim}{t}_1$ and $\underset{\sim}{t}_2$ are directed along the principal axes of curvature (in the circumferential and longitudinal directions) on the ith layer of a through-wall segment at this site. The surface normal $\underset{\sim}{n}$ is perpendicular to the tangent plane containing $\underset{\sim}{t}_1$ and $\underset{\sim}{t}_2$.
(B) shows a myocardial fiber C passing through a point P on the ith surface S. $\underset{\sim}{t}$ is the tangent to C at P. $\underset{\sim}{N}$ is the principal normal of C at P and makes an angle ϕ with the surface normal $\underset{\sim}{n}$.
(C) shows an arbitrary fiber in the ith layer, the principal radii of curvature of the layer, and various stress components of the layer. The subscripts for the shearing stresses are used in the following sense: σ_{12} implies stress acting on the circumferential plane in the longitudinal direction. It can be shown that $\sigma_{12} = \sigma_{21}$.
(D) shows an element of the fiber with various forces acting on it. The element undergoes an acceleration $\ddot{y}_8$ under the action of radial forces N and $(N - \Delta N)$, and axial forces $\tau \Delta h \Delta w$. (E) shows the latitudinal arc lengths, $d_{1,i}$, etc. of three adjacent layers of a through-wall equatorial (site 1) segment along with their radii $r_{1,i}$, etc.

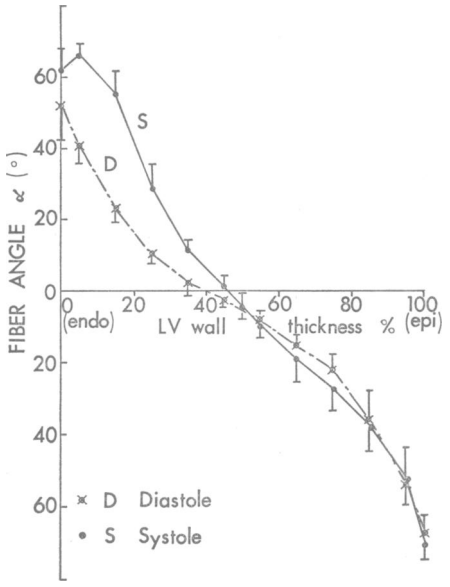

FIGURE 3 Average values of fiber angle ±SEM through the LV wall for the hearts used in this study.

$r_{2,i}$ were then compared with those obtained by direct interpolation between $r_{1,i}$ and $r_{1,n}$ and $r_{2,1}$ and $r_{2,n}$. As the interpolation procedure gave results differing from direct calculation by less than 4%, the simpler interpolation procedure was used in all cases including ellipsoid and measured data.

Fiber Curvature

The curvature k for the fiber in each of the ten nested shells representing the LV wall was calculated by

$$k = k_1 \cos^2 \alpha + k_2 \sin^2 \alpha, \qquad (3)$$

where k_1 and k_2 are reciprocals of r_1 and r_2. Both the measured and ellipsoid values of r_1 and r_2 and the corresponding local values of the fiber angle α near site 1 in each heart, were used for this purpose. The average values of α for the hearts used in this study are shown in Fig. 3.

Surface Areas of Successive Layers of the Myocardium

Computation of stress distributions through the LV wall requires a knowledge of surface areas of each successive layer of a segment in the myocardial wall (see Fig. 2A). The surface areas can be computed from values of arc lengths in latitudinal and longitudinal directions. To account for sequential changes in arc lengths (see Fig. 2E), we need to introduce the following symbols:

$d_{1,i}$ = latitudinal dimension of the ith layer.
$d_{2,i}$ = longitudinal dimension of the ith layer.
$g_{1,i} = d_{1,i}/d_{1,m}$.

$g_{2,i} = d_{2,i}/d_{2,m}$.

$g_i = g_{1,i}g_{2,i}$.

Note that $g_{1,i}$ and $g_{2,i}$ are the normalized latitudinal and longitudinal dimensions of the ith layer; they are normalized with respect to the corresponding dimensions in the middle of the LV wall. Thus g_i is the area of the surface of the ith layer normalized with respect to a similar surface in the middle of the LV wall. $g_{1,i}$ and $g_{2,i}$ were evaluated at site 1 in each heart by

$$g_{1,i} \simeq \prod_{k=1}^{i-1} \frac{(r_{1,k}) + \Delta h}{r_{1,k}} \Big/ \prod_{k=1}^{m-1} \frac{(r_{1,k}) + \Delta h}{r_{1,k}}, \qquad (4)^{3}$$

where Δh is the thickness of a layer, m denotes the value of i at middle layer, and $\prod$ is the product symbol. The iterative procedure for $g_{2,i}$ is the same as that for $g_{1,i}$ except that the first subscript is replaced by 2. For details of derivation of equation 4 see Streeter (1969).

Fiber Stress

The fiber stress, τ_i, acts in the line of each fiber through the wall. The average fiber stress in the wall may be defined as

$$\bar{\tau} = \frac{1}{n-1} \sum_{i=1}^{n-1} \tau_i, \qquad (5)$$

where 1 is the endocardial layer and $n - 1$ is the epicardial layer. Thus $\bar{\tau}$ is the average magnitude of all τ_i in terms of which we define the normalized stress distribution $a_i = \tau_i/\bar{\tau}$

The stress distribution across each layer of wall thickness was assumed as unity (i.e all. fibers through the wall were assumed to have equal stress) for both diastole and systole. This corresponds to assuming a_i to have a constant value unity. In addition, an attempt was made to take into account variable fiber stress due to variation in sarcomere length through the LV wall at end systole. For this purpose variable values of a_i were calculated from isometric sarcomere length-tension data of Sonnenblick for cat papillary muscle (Sonnenblick, 1962) using midwall end systolic sarcomere lengths for each of these hearts (Sonnenblick et al., 1967) and estimated through-wall sarcomere length distributions from the data of Spotnitz, Sonnenblick, and Spiro, (1966). In each heart the average fiber stress $\bar{\tau}$, was then computed by

$$\bar{\tau} = p_1 g_1/(\Delta h \sum_{i=1}^{n-1} a_i k_i g_i), \qquad (6)$$

where p_1 is the endocardial pressure.

Stress Distribution

The pressure or radial stress distribution, p_i, across the LV wall in each heart was then computed from

$$p_i = \frac{\bar{\tau}\Delta h}{g_i} \sum_{j=i}^{n-1} a_j k_j g_j . \qquad (7)$$

[3] Equation 4 is valid for $i > 1$. For the special case $i = 1$,

$$g_{1,1} \simeq 1 \Big/ \left(\prod_{k=1}^{m-1} \frac{(r_{1,k}) + \Delta h}{r_{1,k}} \right)$$

The circumferential ($\sigma_{1,i}$), longitudinal ($\sigma_{2,i}$), and shearing ($\sigma_{12,i}$) stress distributions were computed from

$$\sigma_{1,\,i} = \tau_i \cos^2 \alpha_i \tag{8}$$

$$\sigma_{2,\,i} = \tau_i \sin^2 \alpha_i \tag{9}$$

$$\sigma_{12,\,i} = \tau_i \sin \alpha_i \cos \alpha_i . \tag{10}$$

Total Force in Circumferential Direction

The total force in the circumferential direction per unit longitudinal arc length of the ventricular wall was computed from

$$F_1 = \Delta h \sum_{i=1}^{n-1} \sigma_{1,\,i}\, g_{2,\,i} . \tag{11}$$

RESULTS AND DISCUSSION

The averaged data from five hearts fixed at end diastole and five hearts fixed at end systole are summarized in Table I. Part A shows measured dimensions, R and Z, of ellipsoids of revolution for the endocardial and epicardial surfaces. The values of z, locating site 1 on the latitude (see Fig. 2A) are also included. The small values of z imply that site 1 was near the equator in each heart since for a site exactly at the equator z equals zero. Part B shows the principal radii of curvature of site 1 computed from the data of part A (ellipsoid data). Part C shows the principal radii of curvature of site 1 obtained by direct template measurements (measured data). The indicated increases in wall thickness of 20–30% from diastole to systole are in agreement with those reported by others by direct measurement (Feigl and Fry, 1964). The much larger increases in wall thickness during cardiac contraction (of the order of 100%), reported by some using X-ray techniques (Eber, Greenberg, Cooke, and Gorlin, 1969) are perhaps due to underestimation of the inner systolic diameter resulting from poor definition of the bottoms of the furrows between endocardial protrusions.

Fiber Curvature

The fiber curvature, k, is plotted as a function of LV wall thickness in Fig. 4 from both measured and ellipsoid data for the hearts fixed at end diastole and end systole. The curvatures based on measured data agree well with the ellipsoid data. In systole the fiber curvatures are maximum near the midwall; in diastole they are maximum at a point midway between the endocardium and the midwall. Observe that the fiber curvature in systole is lower than that in diastole near the endocardial surface, and greater in the midwall region. This systolic dip in the curvature reflects the greater values of fiber angle, α, found near the endocardial surface at end systole (Fig. 3).

TABLE I

SUMMARY OF DATA FROM FIVE HEARTS ARRESTED AT END DIASTOLE (D) AND FIVE AT END SYSTOLE (S)

	Cardiac cycle	Endocardial surface	Epicardial surface	Wall thickness
A. Ellipsoid dimensions (measured):				
R (*cm*)	D	1.91 (± 0.101)	2.84 (±0.102)	
	S	1.37 (± 0.025)	2.58 (±0.067)	
Z (*cm*)	D	4.18 (± 0.261)	4.74 (±0.225)	
	S	4.01 (± 0.113)	4.52 (±0.074)	
z (*cm*)	D	0.15 (± 0.25)	0.05 (±0.38)	
	S	0.09 (± 0.09)	0.09 (±0.09)	
B. Ellipsoid data (computed from A):				
r_1 (*cm*)	D	1.90 (± 0.091)	2.82 (±0.095)	
	S	1.36 (± 0.029)	2.57 (±0.066)	
r_2 (*cm*)	D	9.29 (± 1.32)	7.91 (±0.97)	
	S	11.52 (± 0.47)	7.78 (±0.045)	
h (*cm*)	D			0.92 (±0.106)
	S			1.20 (±0.043)
	Increase			30%
C. Measured data (by template):				
r_1 (*cm*)	D	2.15 (± 0.33)	2.87 (±0.21)	
	S	1.19 (± 0.181)	2.74 (±0.188)	
r_2 (*cm*)	D	20.63 (±10.43)	6.20 (±0.84)	
	S	20.73 (±10.78)	8.46 (±1.86)	
h (*cm*)	D			1.02 (±0.062)
	S			1.27 (±0.060)
	Increase			24%

R = minor semiaxis of the ellipsoid.
Z = major semiaxis of the ellipsoid.
z = axial distance from the equatorial plane to the local site of measurement.
r_1 = principal radius of curvature at a local site in the circumferential (latitudinal) direction.
r_2 = principal radius of curvature at the local site in the meridianal (longitudinal) direction.
h = wall thickness.
Average data ±SEM are shown.

Latitudinal and Longitudinal Arc Lengths

As one proceeds through the wall from endocardium to epicardium the normalized surface areas, g_i, increase. This is due to the increase in arc lengths, $g_{1,i}$ and $g_{2,i}$, as seen in Fig. 5. Since the curvature in the circumferential direction is larger than that in the longitudinal direction, $g_{1,i}$ varies more through the wall than $g_{2,i}$, particularly at end systole. Note that the arc lengths from the measured and the ellipsoid data are very similar.

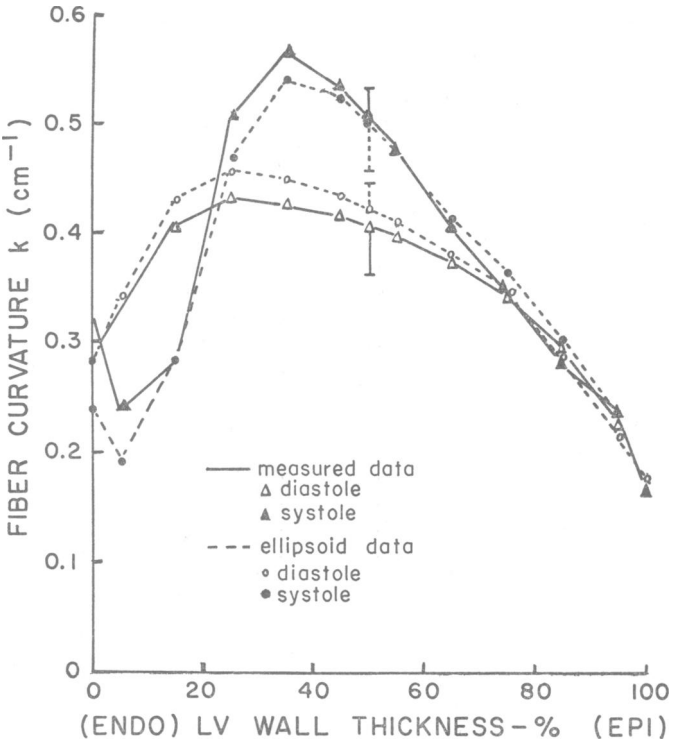

FIGURE 4 Fiber curvature of site 1 through the LV wall, based on measured data and ellipsoid data for hearts stopped at end diastole and at end systole. The average value of the SEM through the wall is shown; the SEM for all curves ranges from 0.009 to 0.120 cm^{-1}.

Pressure or Radial Stress Distribution through LV Wall

The pressure or radial stress distribution normalized by the average fiber stress, $\bar{\tau}$, across the wall thickness, is shown in Fig. 6 for both measured and ellipsoid data. Panels D and S show data for end diastole and end systole based on the fiber stress being constant throughout the wall. Whereas this assumption may be justified in diastole it is questionable at end systole since the fiber tension at end systole may vary through the wall (Hort, 1960; Spotnitz et al., 1966). The determination of systolic tension in actively contracting fibers is a function of instantaneous fiber length and shortening velocity (Fry, 1962; Fry, Griggs, and Greenfield, 1964). Although an upper limit of active tension can be defined by isometric length-tension curves, this upper limit will not be attained during ejecting systole where significant fiber shortening occurs (Spotnitz et al., 1966). However, at end systole, where shortening ceases, fiber tension may become a function of sarcomere length and the isometric length-tension relationship (Taylor, Covell, and Ross, 1969). An illustrative example of the effect of variable fiber stress through the wall at end

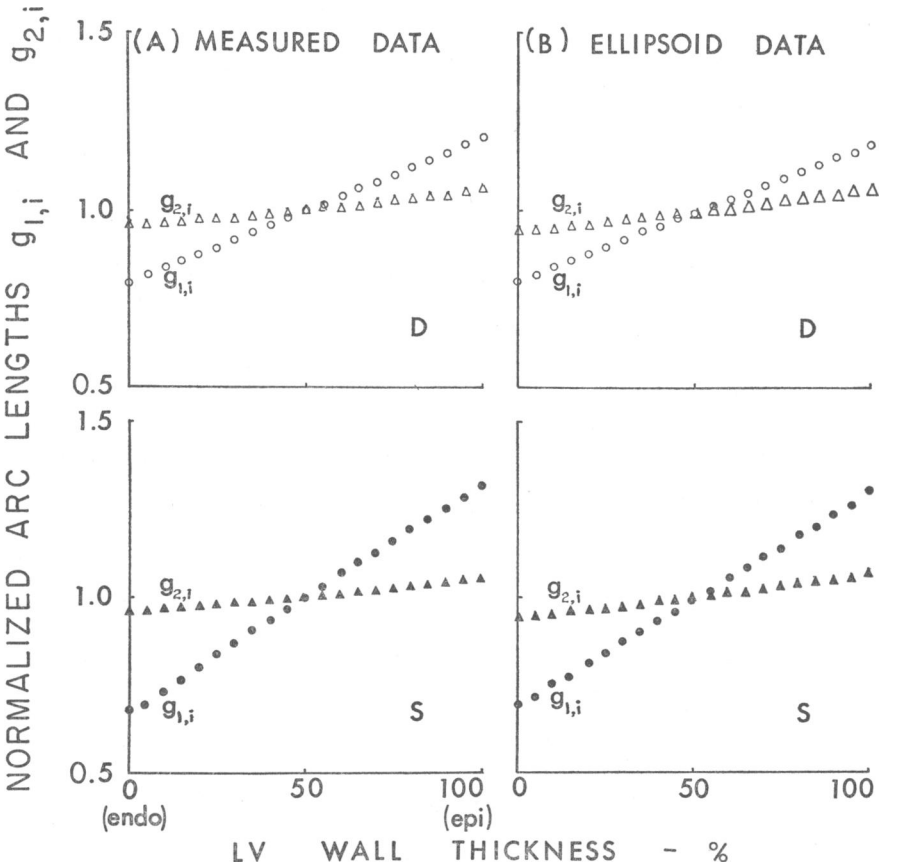

FIGURE 5 Arc lengths in the principal directions at site 1, normalized with respect to the midwall arc lengths; $g_{1,i}$ is along the line of latitude and $g_{2,i}$ is along the line of longitude. Panel A shows arc lengths based on values of principal radii of curvature which were directly measured or interpolated therefrom (measured data). Panel B shows the corresponding values calculated from the semiaxes of the endocardial and epicardial ellipsoids of revolution or interpolated therefrom (ellipsoid data). Data obtained from hearts stopped at end diastole (D) and at end systole (S) are contrasted. SEM for all curves ranges from 0.001 to 0.032.

systole was thus prepared as described in the Methods section. The normalized pressure distribution based on this appears in panel S* of Fig. 6.

In each of these panels only negligible differences appear between the measured and ellipsoid data. In panels D and S the pressure decreases less rapidly as one approaches the epicardium. In panel S* the pressure decreases in an approximately linear manner across the wall. Therefore, the pressure gradients near the epicardial surface are greater in panel S* than in panel S. This is due to the expected increase in fiber tension which accompanies the observed increase in sarcomere length in

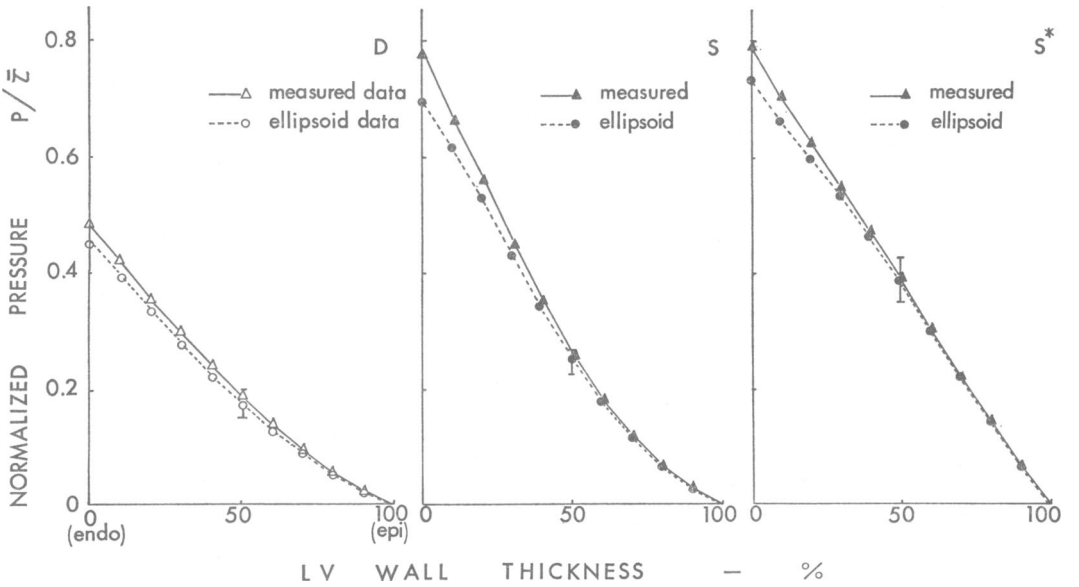

FIGURE 6 Pressure or radial stress distribution across the LV wall, normalized with respect to the average fiber stress $\bar{\tau}$. The average value of the SEM through the wall is shown; the SEM for all curves ranges from 0.004 to 0.086. D = end diastole. S = end systole assuming constant fiber stress through the wall. S* = end systole assuming variable fiber stress through the wall. The average fiber stress, $\bar{\tau}$, in diastole (panel D) was 25.5 (±8.8 SEM) for measured data and 29.1 (±10.3) g/cm² for ellipsoid data, with a mean filling pressure of 11 (±3) g/cm². Under the assumption of constant fiber tension at end systole (panel S) $\bar{\tau}$ was 190.6 (±17.8) for measured data and 209.9 (±16.3) g/cm² for ellipsoid data, the end systolic pressure averaging 143 (±3) g/cm². For the variable fiber tension distribution (panel S*) $\bar{\tau}$ was 184.8 (±15.6) and 206.3 (±28.8) g/cm² for measured and ellipsoid data, respectively.

systole as the wall is traversed toward the epicardium. Such a distribution in fiber tension was predicted by Rushmer and Thal (1951).

Circumferential, Longitudinal, and Shearing Stress Distributions

The distribution of normal stresses in the circumferential and longitudinal directions, as well as the shearing stress through the wall for measured data[4] are shown in Fig. 7. The data were normalized by the average fiber stress $\bar{\tau}$. At end diastole (panel D) the circumferential stresses predominate in the middle 80% of the wall; the longitudinal stresses predominate in the outer 20%; and shear stresses predominate near the outer two faces of the wall changing sign at midwall. At end systole, if a constant fiber stress is assumed (panel S), all three stress distributions

[4] It can be shown that the various stress distributions for the ellipsoid data would be very similar, since their computation is based on values of fiber curvatures and arc lengths shown in Figs. 4 and 5. Therefore, for clarity, stress distributions for the ellipsoid data were not included in Fig. 7.

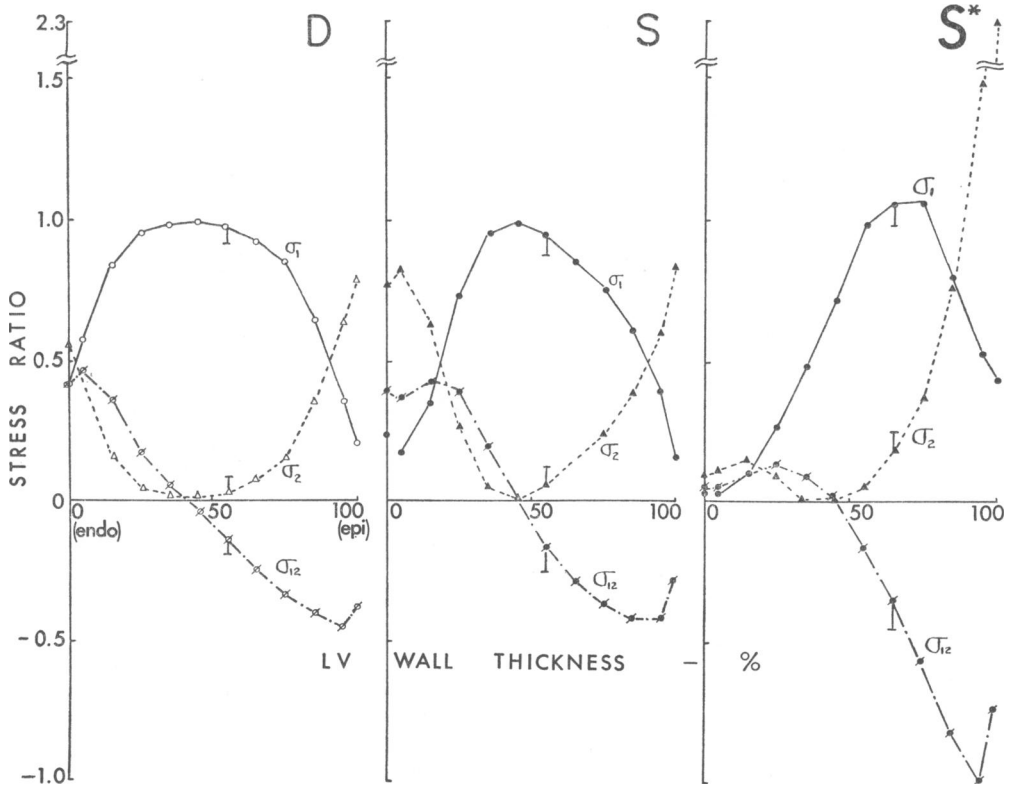

FIGURE 7 Stress distribution through the LV wall normalized with respect to the average fiber stress $\bar{\tau}$. The average of the SEM through the wall is shown; the SEM for curves in panels D and S range from 0.003 to 0.134; in panel S* they range from 0.0002 to 0.650. σ_1 = circumferential stress component. σ_2 = longitudinal stress component. σ_{12} = shearing stress in the longitudinal direction acting on a plane perpendicular to the circumferential direction. D = end diastole. S = end systole assuming constant fiber stress through the wall. S* = end systole assuming variable fiber stress through the wall. $\bar{\tau}$'s for each panel are the same as in Fig. 6.

are comparable to those obtained for end diastole (panel D). However, for the variable fiber stress distribution assumed above (panel S*), the three stress distributions are magnified toward the epicardium. As mentioned in the Appendix, in all stress calculations the contribution of the force of radial acceleration was neglected. This would tend to change the myocardial stress components σ_1, σ_2, σ_{12}, at the end systole, by a negligible amount; it will not change the shape of the curves in Fig. 7.

Comparison with Force Gauge Data

A comparison of the predicted force, F_1, in the circumferential direction per unit longitudinal arc length of the ventricular wall, using both measured and ellipsoid

TABLE II

FORCE IN CIRCUMFERENTIAL DIRECTION PER UNIT LONGITUDINAL ARC LENGTH (G/CM)

Comparison of the predicted forces from the present study with directly recorded data of Greenfield.
All data are corrected for the differences in LV wall thickness.

	D	S	S*
Measured data	12.7	103.1	89.5
Ellipsoid data	14.5	113.4	100.0
Force gauge data	12.5	99.5	

data in equation 11, was made with experimental data from a dog heart supplied by Dr. Joseph C. Greenfield, Jr., of Duke University. These data were obtained by using an auxotonic force transducer developed by Feigl, Simon, and Fry (1967), which was implanted in the free wall of a dog's left ventricle. Table II shows that the circumferential force developed in the auxotonic force gauge is close to that predicted by our study for end diastole and end systole.

Comparison with Data in the Literature

In a number of papers (Johnson and DiPalma, 1939; Gregg and Eckstein, 1941, Salisbury, Cross, and Rieben, 1962; Kreuzer and Schoeppe, 1963; Kirk and Honig; 1964; Shenderov, Taraeva, and Mdinaradze, 1967) intramyocardial pressure peaks exceeding the pressure in the LV cavity have been reported. Such pressure peaks could arise if the fiber curvature at the local site within the LV wall is negative either in its physiologic state or due to the experimental technique used for measuring pressure. We did not see these pressure peaks in the present study since local sites with negative fiber curvature (e.g. on trabecular infoldings) were specifically avoided. In one heart, however, such a site was studied (Streeter, 1969) and an intramyocardial pressure peak was estimated near the endocardium.

Our stress distributions through the LV wall as seen in Figs. 6 and 7 may be compared with those of Wong and Rautaharju (Fig. 5 in Wong and Rautaharju, 1968). Although their pressure or radial stress distribution is similar to ours, their circumferential and longitudinal stress distributions are not; theirs peak at the endocardial surface. This is not surprising since these authors did not take into account the orientation of muscle fibers through the wall, and the circumferential and longitudinal stress distributions are very sensitive to fiber orientation. The radial stress distribution, however, is essentially dependent upon the principal curvatures of the LV wall.

CONCLUSION

In conclusion (*a*) a method is presented for thick wall stress analysis based on actual measurements of wall curvatures and fiber orientation through the LV wall in

canine hearts. Although the present analysis is restricted to end diastole and end systole, theory is developed to include the dynamic aspects of the entire cardiac cyle and sequential fiber activation through the wall when appropriate experimental data become available. (*b*) The general agreement is good between ellipsoid data and measured data in calculation of various parameters (e.g. curvature, grid spacings, stress distributions, and circumferential wall tension as seen in Figs. 4–6 and Table II). It lends support to the use of ellipsoid data which are relatively easy to acquire and tend to smooth out local curvature variations in favor of the gross morphology of the left ventricle. (*c*) These data will be helpful in modeling the heart in a realistic fashion for application in understanding the physiology of ventricular function and should permit analysis of the mechanical behavior of the coronary vascular bed since the small coronary blood vessels are embedded in the myocardial wall.

APPENDIX

Geometry of Myocardial Fibers and Surfaces

To appreciate the details of computation of fiber curvature from directly measurable data, it is necessary to understand a few concepts from the differential geometry of curves and surfaces (Hilbert and Cohn-Vossen, 1952; Struik, 1961). Consider a segment S of a myocardial surface with a muscle fiber C in it (see Fig. 2B). The limiting direction of the line joining a point P on C with an adjacent point on C is called the *tangent* to C at P. The plane that contains the local arc of C at P is called the *osculating plane* of C at P. The line $\underset{\sim}{\mathrm{N}}$ in the osculating plane at P which is also perpendicular to $\underset{\sim}{\mathrm{t}}$ is called the *principal normal* to C at P. There are infinitely many curves like C which pass through P and have $\underset{\sim}{\mathrm{t}}$ as their common tangent and lie on S. They all have different principal normals at P. Among all such curves at P in the direction of $\underset{\sim}{\mathrm{t}}$, there is a curve C' which has the smallest curvature. This curve C' is called the *normal section* of S at P in the direction $\underset{\sim}{\mathrm{t}}$, because the principal normal $\underset{\sim}{\mathrm{N}}$ of C' is the same as the surface normal $\underset{\sim}{\mathrm{n}}$ at P. If the curvature of C' is k_n, and the angle that the principal normal $\underset{\sim}{\mathrm{N}}$ of C makes with $\underset{\sim}{\mathrm{n}}$ is ϕ, then, according to a theorem due to Meusnier (Struik, 1961),

$$k = k_n \sec \phi, \tag{1A}$$

where k is the curvature of the fiber C. Physically these concepts can be visualized by imagining a small arc of a semiflexible wire constrained to lie on a smooth surface. In order to keep the wire always in contact with the surface while rotating about its tangent, it must be flexed. It will be found that the curvature of the wire arc will be the least (configuration C') when the plane of the wire arc is perpendicular to the tangent plane of the surface.

If we now compare the curvature k_n of the infinitely many normal sections of S at P in the directions such as $\underset{\sim}{\mathrm{t}}$, we should find two orthogonal directions $\underset{\sim}{\mathrm{t}}_1$ and $\underset{\sim}{\mathrm{t}}_2$ where the curvatures of the normal sections C_1' and C_2' are extreme, one being the maximum and the other the minimum. These curvatures, k_1 and k_2, are called the *principal curvatures* of the surface S at P. If the direction $\underset{\sim}{\mathrm{t}}$ makes an angle α with the direction $\underset{\sim}{\mathrm{t}}_1$ then the curvature k_n of the normal section C' in the direction $\underset{\sim}{\mathrm{t}}$ is given by Euler's theorem (Struik, 1961) as

$$k_n = k_1 \cos^2 \alpha + k_2 \sin^2 \alpha. \tag{2A}$$

If the wire arc referred to above is in configuration C' with its plane normal to the tangent plane of the surface, and if we rotate its plane about the surface normal keeping the wire in contact with the surface, the curvature k_n of the wire arc will be found to change. It will assume its extreme values in configurations C_1' and C_2'.

Thus, for an arbitrary configuration C of a muscle fiber the curvature k can be obtained by using equations 1A and 2A. The determination of k for an endocardial or epicardial muscle fiber then requires knowledge of k_1, k_2, α and ϕ. It is difficult to measure ϕ. However, it is reasonable to assume that $\phi = 0$, since a stressed fiber joining two points and constrained to remain on a shell surface but unconstrained otherwise, would tend to assume a geodesic configuration; for a geodesic it can be shown (Struik, 1961) that ϕ is zero. Thus, for superficial myocardial fibers, curvature can be determined by measuring the principal curvatures k_1 and k_2 and the fiber angle α. Then equation 2A takes the form

$$k = k_1 \cos^2 \alpha + k_2 \sin^2 \alpha. \tag{3A}$$

For a fiber that is not either on the endocardial or the epicardial surface, evaluation of k needs further assumptions. To that end we idealize the myocardial surfaces as two truncated ellipsoids of revolution (see Fig. 2A), with semiaxes R and Z. We further postulate that the internal fibers lie on a set of nested ellipsoids of revolution bounded by the endocardial and epicardial surfaces of this set. Since the internal fibers are also constrained to remain on shell surfaces, ϕ will be zero. Let us also assume that R and Z for the intermediate ellipsoids, are obtainable by linear interpolation between their values at the surfaces. Using the measured surface values as well as interpolated values of R and Z, we can calculate the principal radii of curvature r_1 and r_2 for the surfaces and the intermediate layers of the wall at any local site (e.g. site 1) from

$$r_1 = (Z^2 - [Z^2 - R^2] f^2)^{1/2} R/Z \tag{4A}$$

$$r_2 = (Z^2 - [Z^2 - R^2] f^2)^{3/2}/RZ, \tag{5A}$$

where $f = z/Z$ and z is the site dimension determining the location of the latitude of the point at site 1. The values of r_1 and r_2 so obtained can then be used in equation 3A together with the fiber angle data through the wall at the site to provide an estimate of the curvature of a muscle fiber.

Equilibrium Considerations

Having developed the method for computing the curvature of a myocardial fiber, we can use the computed curvature to relate the forces acting on a fiber to the stress in the fiber. Consider the equilibrium of an arc of a fiber as shown in Fig. 2D. Erect a local right-handed rectangular coordinate system with axis y_1 along the tangent to the fiber arc, y_2 perpendicular to the osculating plane, and y_3 along the principal normal. For the assumed model of the myocardium, the following forces are acting on the fiber segment: forces $N - \Delta N$ and N on the epicardial and the endocardial surfaces respectively, the axial forces $\tau \Delta h \Delta w$, and the force of radial acceleration, $\rho \ddot{y}_3 \Delta h \Delta w \Delta l$, where Δh, Δw and Δl are the dimensions of the fiber as shown, ρ is mass density of the fiber material, and $\ddot{y}_3$ is the radial acceleration of the mass center of the fiber arc. For equilibrium in the y_3 direction,

$$\Delta N = \Delta v (k\tau + \rho \ddot{y}_3), \tag{6A}$$

where $\Delta v = \Delta h \Delta w \Delta l$ is the volume of the infinitesimally long arc of the fiber, and k is the curvature. Equilibrium equations for the other two directions are identically satisfied. Now if the inertial forces are neglected then equation 6A becomes

$$\Delta N = \Delta v k \tau. \tag{7A}$$

To facilitate the summation of force increments ΔN through the layers of a wall segment, consider a set of nested shell layers with local normal $\underset{\sim}{n}$ (Fig. 2A and 2C) along which ΔN is directed. The bounding set of longitudinal and latitudinal surfaces, which contain this normal will be orthogonal to each of the nested shell surfaces, making a triply orthogonal set of surfaces[5] (Struik, 1961). The ith layer of the segment in Figures 2A and 2C is thus bounded by a triply orthogonal set of surfaces. For an element of the ith layer equation 7A becomes

$$\Delta N_i = k_i a_i g_i \, \Delta h \, \bar{\tau} \, d_{1,m} \, d_{2,m} , \tag{8A}$$

where Δh is the thickness of the layer, and k_i, a_i, g_i, $d_{1,m}$ and $d_{2,m}$ are as defined in the text previously. If p_1 and p_n are the endocardial and the epicardial pressures respectively, the excess of the endocardial force $N_1 = p_1 g_1 \, d_{1,m} \, d_{2,m}$ over the epicardial force $N_n = p_n g_n \, d_{1,m} \, d_{2,m}$ can be obtained by summing the force differentials ΔN_i for all the $n - 1$ layers. Thus, by equation 8A

$$\begin{aligned} N_1 - N_n &= (p_1 g_1 - p_n g_n) \, d_{1,m} \, d_{2,m} \\ &= \bar{\tau} \, \Delta h \sum_{i=1}^{n-1} k_i a_i g_i \, d_{1,m} \, d_{2,m} . \end{aligned} \tag{9A}$$

Now if the epicardial pressure $p_n = 0$, then

$$\bar{\tau} = p_1 g_1 \Big/ \left(\Delta h \sum_{i=1}^{n-1} a_i \, k_i \, g_i \right). \tag{10A}$$

Thus, $\bar{\tau}$ can be computed only if the myocardial fiber stress distribution as typified by a_i is known. For a given site the geometric quantities $d_{1,i}$, $d_{2,i}$, $g_{1,i}$, $g_{2,i}$, and g_i can be determined numerically from a knowledge of the local principal radii of curvature and the layer thicknesses. This computational procedure is outlined by Streeter (1969).

Once $\bar{\tau}$ is computed using equation 10A, the distribution of stresses can be found. The pressure distribution p_i through the myocardial wall is given by

$$p_i = \frac{\bar{\tau} \Delta h}{g_i} \sum_{j=i}^{n-1} a_j \, k_j \, g_j . \tag{11A}$$

Finally, it is of interest to compute the distribution of wall tensions in a chosen direction. This can be found in the following manner. Let us consider the fibers in the ith layer of a through-wall segment of the triply orthogonal grid. If a triangular lamina is taken out of the ith layer so that the face of the hypotenuse is normal to the direction of the fibers and the other two faces are normal to the lines of latitude and longitude, then by elementary equilib-

[5] All three pairs of surfaces, e.g. longitudinal, latitudinal, and the myocardial surfaces, intersect locally at right angles with each other.

rium considerations it can be shown (Timoshenko and Goodier, 1951; Biot, 1965) that

$$\sigma_{1,i} = \tau_i \cos^2 \alpha_i \quad (12A)$$

$$\sigma_{2,i} = \tau_i \sin^2 \alpha_i \quad (13A)$$

$$\sigma_{12,i} = \tau_i \sin \alpha_i \cos \alpha_i , \quad (14A)$$

where $\sigma_{1,i}$ = normal stress on a plane perpendicular to the line of latitude in the ith layer, $\sigma_{2,i}$ = normal stress on a plane perpendicular to the line of longitude in the ith layer and $\sigma_{12,i}$ = shear stress on these planes in the ith layer.

The total force, F_1, in the circumferential direction per unit longitudinal arc length of the ventricular wall can be computed from

$$F_1 = \Delta h \sum_{i=1}^{n-1} \sigma_{1,i} \, g_{2,i} . \quad (15A)$$

Similarly the total force, F_2, in the longitudinal direction per unit circumferential arc length of the ventricular wall can also be computed. It may be pointed out that equations 3A, 4A, 5A, 10A, 11A, 12A, 13A, 14A, and 15A are respectively the same as equations 3, 1, 2, 6, 7, 8, 9, 10, and 11 in the text.

We are grateful to Dr. D. L. Fry for his help and criticism.
We also thank Virginia M. Fry and Stewart Leavitt for the art work, and Sam Silverman for photography.

Part of this report was submitted by Dr. Streeter to The Catholic University in partial fulfillment of the requirements of the degree of Doctor of Philosophy (Biomechanics).

This work was supported in part by U. S. Public Health Service Research Grant HE 5454-08 from the National Heart Institute and National Science Foundation Research Grant GK-2802.

Received for publication 22 August 1969 and in revised form 20 November 1969.

REFERENCES

BIOT, M. A. 1965. Mechanics of Incremental Deformations. John Wiley and Sons, Inc., New York. 24.
BURTON, A. C. 1957. *Amer. Heart J.* **54**:801.
EBER, L. M., H. M. GREENBERG, J. M. COOKE, and R. GORLIN. 1969. *Circulation.* **39**:455.
FEIGL, E. O., and D. L. FRY. 1964. *Circ. Res.* **14**:541.
FEIGL, E. O., G. A. SIMON, and D. L. FRY. 1967. *J. Appl. Physiol.* **23**:597.
FRY, D. L. 1962. *Fed. Proc.* **21**:991.
FRY, D. L., D. M. GRIGGS, JR., and J. C. GREENFIELD, JR. 1964. *Circ. Res.* **14**:73.
GREGG, D. E., and R. W. ECKSTEIN. 1941. *Amer. J. Physiol.* **132**:781.
HILBERT, D., and S. COHN-VOSSEN. 1952. Geometry and Imagination. [Translation.] Chelsea Publishing Co., New York.
HOOD, W. P., JR., W. J. THOMPSON, C. E. RACKLEY, and E. L. ROLETT. 1969. *Cir. Res.* **24**:575.
HORT, W. 1960. *Virchows Arch. Abt. A. Pathol. Anat.* **333**:523.
JOHNSON, J. R., and J. R. DIPALMA. 1939. *Amer. J. Physiol.* **125**:234.
KIRK, E. S., and C. R. HONIG. 1964. *Amer. J. Physiol.* **207**:361.
KREUZER, H., and W. SCHOEPPE. 1963. *Arch. Gesamte Physiol. Menschen Tiere (Pfluegers).* **278**:181.
ROSS, J., JR., E. H. SONNENBLICK, J. W. COVELL, G. A. KAISER, and D. SPIRO. 1967. Circ. Res. **21**:409.
RUSHMER, R. F., and N. THAL. 1951. *Circulation.* **4**:219.

SALISBURY, P. F., C. E. CROSS, and P. A. RIEBEN. 1962. *Circ. Res.* **10**:608.
SANDLER, H., and H. T. DODGE. 1963. *Circ. Res.* **13**:91.
SHENDEROV, D. M., N. G. TARAEVA, and YU. S. MDINARADZE. 1967. *Bull. Exp. Biol. Med.* **64**:1042.
SONNENBLICK. E. H. 1962. *Fed. Proc.* **21**:975.
SONNENBLICK, E. H., J. ROSS, JR., J. W. COVELL, H. M. SPOTNITZ, and D. SPIRO. 1967. *Circ. Res.* **21**:423.
SPOTNITZ, H. M., E. H. SONNENBLICK, and D. SPIRO. 1966. *Circ. Res.* **18**:49.
STREETER, D. D., JR., and D. L. BASSETT. 1966. *Anat. Rec.* **155**:503.
STREETER, D. D., JR., H. M. SPOTNITZ, D. J. PATEL, J. ROSS, JR., and E. H. SONNENBLICK. 1969. *Circ. Res.* **24**:339.
STREETER, D. D., JR. 1969. A rational model for myocardial stress analysis based on fiber orientation and curvature. Ph.D. Thesis. The Catholic University of America, Washington.
STRUIK, D. J. 1961. Lectures on Classical Differential Geometry. Addison-Wesley Publishing Co., Inc., Reading, Mass. 2nd edition. 76, 86, 99, 104, 131, 140.
TAYLOR, R. R., J. W. COVELL, and J. ROSS, JR. 1969. *Amer. J. Physiol.* **216**:1097.
TIMOSHENKO, D., and J. N. GOODIER. 1951. Theory of Elasticity. McGraw-Hill Book Company, New York. 2nd edition. 14.
WOODS, R. H. 1892. *J. Anat. Physiol.* **26**:302.
WONG, A. Y. K., and P. M. RAUTAHARJU. 1968. *Amer. Heart J.* **75**:649.